JOURNAL OF PROPULSION AND POWER
Vol. 9, No. 1, Jan.–Feb. 1993

Advanced Direct-Design Procedure for Centrifugal Impellers

Sarim N. J. Al-Zubaidy*
UAE University, Al-Ain, United Arab Emirates

The design of centrifugal impellers usually starts with a preliminary design making use of one-dimensional flow analysis thus enabling the skeletal dimensions of the impeller to be determined. This is followed by a detailed design that requires the complete description of the three-dimensional geometry which is subsequently modified by means of successive aerodynamic analysis (indirect approach). The initial description of the blade geometry relies heavily on the experience and the engineering judgement of the designer. This article will present a method that will replace this arbitrary stage of the design sequence by a design procedure that will effectively generate the three-dimensional coordinate of impellers designed for a prescribed velocity schedule (direct-design approach). The study suggests that the degree of blade wrapping could—and was controlled by—adjusting the magnitude and the distribution characteristics of the relative pressure loading parameter. The leaning of the mean streamline forward is caused by increasing the loading distribution while a backward lean is achieved by decreasing the blade loading. The rate at which the radial relative velocity accelerates was used to eliminate undesirable blade curvatures during the design procedure.

Nomenclature

B = blockage factor due to blade thickness
b = width
C = absolute velocity
C_n = blade loading coefficient
C_p = specific heat at constant pressure
DR = diffusion ratio
d = diameter
e = inducer-to-tip diameter ratio
f = function of . . . [Eq. (8b)]
h = hub-to-tip diameter ratio
M = Mach number
m = mass flow rate, length along streamline
N = rotational speed
n_b = number of blades
P = pressure
r = radius
T = temperature
W = relative velocity
Z = distance along axis of rotation
α = angle between tangent to meridonal streamline and Z axis (measured from tangential)
β = relative flow angle, blade angle (measured from tangential)
γ = ratio of specific heats
η = efficiency
θ = relative angular coordinate
ρ = density
ϕ_s = slip factor
ω = angular speed of rotation

Subscripts

c = curvature
e = inducer tip condition
m = meridional
p = pressure
r = radial direction
s = suction
w = component in the direction of perpherial velocity
z = axial direction
θ = tangential direction
0 = stagnation condition
1 = impeller inlet condition
2 = impeller exit condition

Received April 18, 1991; revision received April 30, 1992; accepted for publication June 2, 1992.

*Associate Professor, Mechanical Engineering Department.

Introduction

IN order for the design process of radial flow centrifugal impellers to progress beyond the preliminary design stage, a detailed description of the blade geometry is required. The quasi-three-dimensional or three-dimensional flow analysis procedures are basically intended to evaluate the loading distribution and fluid properties within the specified geometry. In general, the great majority of procedures used for the design of radial turbomachinery relies on the indirect approach. In this approach, a preliminary shape of the impeller is arbitrarily specified and the flow within the rotating channels is then analyzed. The velocity profiles obtained will be examined for any irregularities and the initial geometry will be successively modified until an acceptable loading distribution is achieved. The process of continually refining the blade shape is not only time-consuming and expensive in terms of computational cost, but could be very laborious. The alternative approach (which is designing the impeller using a direct procedure) assumes that the acceptable loading distribution is known as a starting point and the aim would be to produce an impeller geometry that would produce the initially prescribed distribution. The resulting geometrical description in this case would be defined by arrays of discrete coordinate points, and therefore, have to be fitted by a suitable three-dimensional curve in order to automate the overall design procedure. The relative merits of employing the direct approach over the indirect approach is shown in Fig. 1.[1] The abscissa represents six impellers (A–F) that have been designed to meet the same performance requirements and to have a similar diffusion schedule. The ordinate represents the time ratio taken by an IBM, series 4331 mainframe computer to achieve the design objectives. It can be deduced from the figure that on average the direct approach requires one seventh the time taken by the indirect approach. Further details may be found in Ref. 1. In spite of the many attractive features of the direct approach, the design sequence of radial turbine rotors and compressor impellers still relies heavily on arbitrary description of blading geometry (indirect-design approach). The purpose of this article is to present a comprehensive aerothermodynamic direct-design procedure for centrifugal impellers. The proposed procedure produced an example design that incorporated indirectly the basic important mecha-

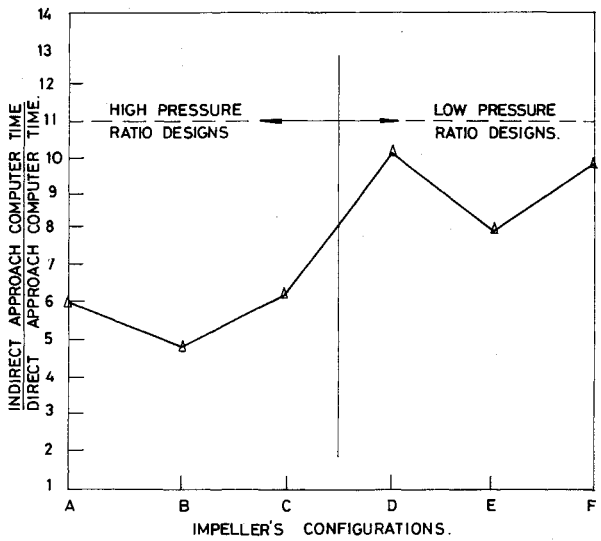

Fig. 1 Saving in computer time when using the direct approach compared with the indirect approach.[1]

From the definition of total-to-total adiabatic efficiency

$$T_{02} = T_{01}\{1 + (1/\eta)[(P_{02}/P_{01})^{(\gamma-1)/\gamma} - 1]\} \quad (4)$$

with the help of the outlet velocity triangle, the following relation could be obtained:

$$\left(\frac{C_2}{\sqrt{C_pT_{02}}}\right) = \left(\pi\frac{d_2N}{\sqrt{C_pT_{01}}}\right) \cdot \sqrt{(2\phi_s - 1) + \left(\frac{(W_2/W_1)(e\tan\beta_e)}{\sin\{\tan^{-1}[\sqrt{2e^2/(e^2+h^2)}\tan\beta_e]\}}\right)^2} \quad (5)$$

$$M_2 = \frac{\frac{C_2}{\sqrt{C_pT_{02}}}}{(\gamma-1)\left[1 - 0.5\left(\frac{C_2}{\sqrt{C_pT_{02}}}\right)^2\right]} \quad (6)$$

Finally, the tip-width to tip-diameter ratio can be shown to be given by the following equation:

$$\frac{b_2}{d_2} = \left(\frac{\gamma-1}{\gamma}\right)\frac{\left(1+\frac{\gamma-1}{\gamma}M_e^2\right)^{1/(\gamma-1)}\left(\frac{1}{\pi^2}\right) + \phi_s\left(\frac{d_2N}{\sqrt{C_pT_{01}}}\right)^2\frac{m\sqrt{C_pT_{01}}}{d_2P_{01}}}{B_2(W_2/W_1)^2[0.5h^2 + e^2(0.5+\tan^2\beta_e)] - (1-\phi_s)^2\left(\frac{P_{02}}{P_{01}}\right)\frac{d_2N}{\sqrt{C_pT_{01}}}} \quad (7)$$

nisms that effect the flow turbulence structure. This was achieved by modifying the blade curvature distribution and the flow rate of turning from inlet to outlet such that the required overall diffusion ratio was achieved.

Evaluation of Overall Dimensions

For a given set of performance requirements, the impeller design problem entails the calculation of the complete geometrical dimensions. It is also necessary to identify the constraints such as stress and temperature or the inducer tip Mach number limits. The geometrical shape of a typical radial flow impeller and the inlet and outlet velocity triangles in addition to the actual compression process are shown in Fig. 2.

By assuming that the whirl inlet absolute velocity to be zero and the whirl outlet velocity component to be equal to $(\phi_s U_2)$ (for radial-bladed impeller), the well-known Euler's equation $C_{w2}, U_2 - C_{w2}U_1 = C_p\Delta T_0$, can be written as follows (further details could be found in Ref. 2):

$$\frac{d_2N}{\sqrt{C_pT_{01}}} = \left(\frac{1}{\pi}\right)\sqrt{\left(\frac{1}{\phi_s\eta}\right)\left[\left(\frac{P_{02}}{P_{01}}\right)^{(\gamma-1)/\gamma} - 1\right]} \quad (1)$$

The following expression for the relative Mach number at the inducer tip can be derived from the inlet velocity vector diagram:

$$M_e^2 = \frac{\left(\pi e\frac{d_2N}{\sqrt{C_pT_{01}}}\right)^2}{(\gamma-1)\left\{1 - \sin^2\beta_e\left[1 + \frac{1}{2}\left(\pi e\frac{d_2N}{\sqrt{C_pT_{01}}}\right)\right]^2\right\}} \quad (2)$$

The application of the continuity and energy equations to the inducer section produces the following equation for the mass flow parameter:

$$\frac{m\sqrt{C_pT_{01}}}{d_2^2P_{01}} = \left(\frac{\pi}{4}\right)\left(\frac{\gamma}{\sqrt{\gamma-1}}\right)B_1\left[\left(\frac{d_e}{d_2}\right)^2 - \left(\frac{d_h}{d_2}\right)^2\right] \cdot \left\{\frac{M_e\sin\beta_e}{\left[1 - \left(\frac{\gamma-1}{2}\right)(M_e\sin\beta_e)^2\right]^{(\gamma+1)/2(\gamma-1)}}\right\} \quad (3)$$

The slip factor (in the above equation) could be expressed in terms of selected design parameters and can be written as

$$\phi_s = \frac{1 \pm \sqrt{1 - \sec^2\alpha_2\left[1 - \left(\frac{d_1}{d_2}\frac{W_2}{W_1}\sec\beta_1\right)^2\right]}}{\sec^2\alpha_2} \quad (8a)$$

or generally as

$$\phi_s = f\left(\alpha_2, \frac{d_1}{d_2}, \frac{W_2}{W_1}, \sec\beta_1\right) \quad (8b)$$

The principal dimensions of the impeller, with the exception of the impeller axial length along its axis of rotation, can be

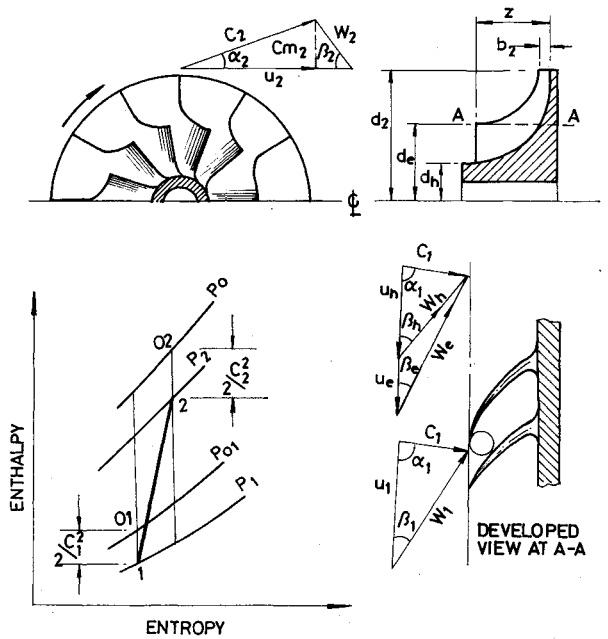

Fig. 2 Three views of centrifugal impeller, inlet and outlet velocity diagrams and description of the compression process.

found by solving Eqs. (1–8) for the principal dimensions and flow boundary conditions (i.e., d_2, b_2, d_e, d_h, β_e, β_2, α_2, etc.) but it is necessary to know the following: 1) design specifications consisting of P_{02}/P_{01}, m and in some cases N; 2) constraints defined by the permissible ranges of M_e, β_e, h, b_2/d_2, and n_b; and 3) initially assumed quantities including ϕ_s, η, B_1, B_2, and W_1/W_2 (or DR).

The evaluation of the impeller principal dimensions is achieved by solving the above-mentioned governing Eqs. (1–8) for the specified design requirements. In this study, the optimum value of the inducer-tip to the impeller-tip diameter ratio was calculated by combining the continuity equation together with Eqs. (2) and (3) and then optimizing the resulting expression for the condition of minimum entry relative Mach number. This condition is described by the following expression which is given in terms of some important selected dimensionless quantities:

$$e = \frac{d_e}{d_2}\left\{\left[\frac{0.57316\left(\frac{\gamma-1}{\gamma}\right)\frac{m\sqrt{C_pT_{01}}}{d_2^2P_{01}}}{\frac{d_2N}{\sqrt{C_pT_{01}}}}\right]^{2/3} + h^2\right\}^{0.5} \qquad (9)$$

Figure 3 shows a comparison between values of parameter "e" calculated using the condition described by Eq. (9) with data from existing designs that have known inlet flow conditions, geometries, and design requirements. Thirteen individual design cases have been considered (data obtained from Refs. 3–10), it can be seen in only one example in all the examined cases in which the value of the parameter e is below the optimum value suggested by the above expression. This particular impeller (case marked no. 1) has a design point rotational speed of 50,000 rpm and an exceptionally high total-to-total pressure ratio of approximately 12:1, whereas in all other examined designs the value of the inducer-to-tip diameter ratio is higher than what the above expression suggests. Two regression polynomials have been fitted through the data [points obtained from the application of Eq. (9) and from readily available data]. It does generally seem that at lower dimensionless mass flow parameter, data from available designs do approximate the suggested optimum value of parameter e which is specified by Eq. (9). However, as the mass flow parameter increases, the deviation from the suggested optimum value increases.

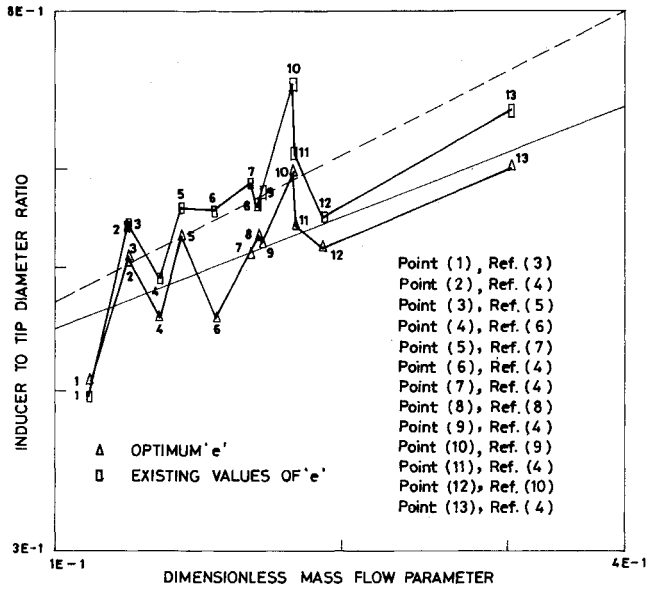

Fig. 3 Comparison between optimum value of e [calculated using Eq. (9)] and of existing designs.

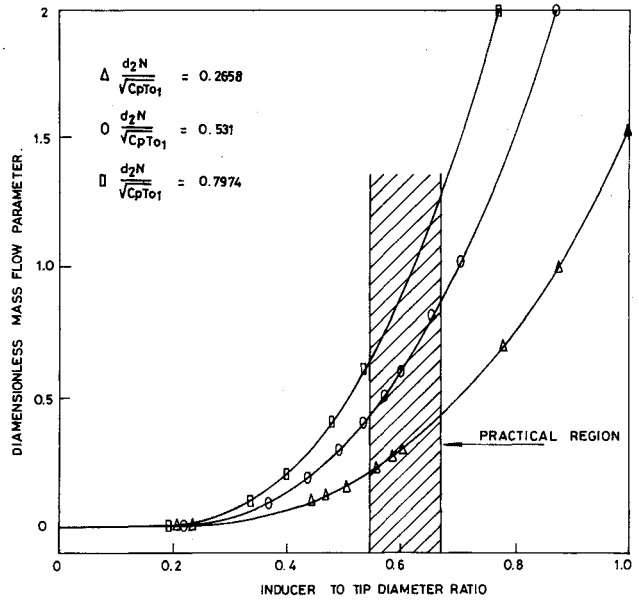

Fig. 4 Effect of rotational speed on the inducer tip diameter and relative entry Mach number.

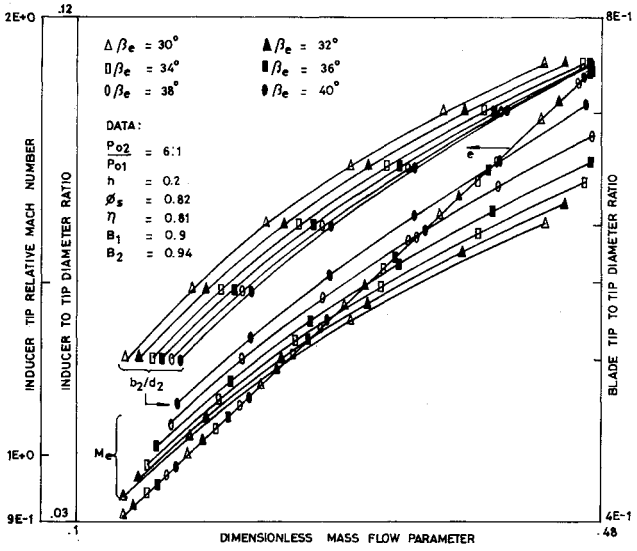

Fig. 5 Possible impeller design chart for specified requirements.

Figure 4 is obtained by solving the above-mentioned condition and it shows the effect of varying the impeller speed on the inducer tip Mach number and the inducer tip diameter for the stated design requirements. It can be seen that the region of minimum Mach number is independent of the speed of rotation. The practical region of the inducer-to-tip diameter ratio is highlighted in Fig. 4. Figure 5 shows a design chart for radial flow centrifugal impellers. For any required total-to-total pressure ratio (taken in the present design to be 6:1), the basic dimensions of the impeller can be evaluated.

Prescribed Mean Streamline Velocity

When the impeller inlet and outlet blade angles are fixed (from the previous design stage), the vane-detailed profile will influence the pressure and velocity distribution throughout the impeller. The arbitrary choice of the geometry of the blades could be overcome by following a direct-design procedure, where the passage is designed to accommodate a prescribed diffusion rate. The overall profile of what is considered to be an acceptable spatial rate of diffusion is beyond the intended scope of this article, but it is well-documented in the open literature (e.g., Refs. 11–13). Since the velocity is initially prescribed along the mean streamline of the impeller,

the general configuration of this line will be dictated by the prescribed velocities. In the following section a brief summary of how the mean streamline was obtained is described.

The relative velocity vector corresponding to the rms diameter at entry, may be resolved into three components in the axial, radial, and tangential directions. In the present design, the radial component at entry has been assigned a minimum value (chosen to have small positive value) and the axial component is assumed maximum. At the outlet, in the case of the example radial flow impeller, the radial component is assumed to attain the maximum value and the axial component attains its minimum value. A mean streamline is defined as a locus of points joining the rms radius at inlet with a point at the outlet radius which bisects the tip width. The constraints imposed on the general shape of this line is that the radial and tangential components must not decelerate to such an extent that the value of the total relative velocity drops below that given by the diffusion criterion.

The spatial description of the mean streamline can then be found by assuming a suitable value for the impeller length along its axis of rotation and then prescribing the component velocities and angles. This was achieved in the present study by an iterative program.

Design Theory

The inviscid equations of motion relative to a rotating impeller in which an axial symmetry is assumed could be written as follows:

$$-\frac{1}{\rho}\frac{\partial P}{\partial r} = \frac{W^2 \cos^2\alpha\beta \cos\alpha}{r_c} + \frac{dW_m}{dm} W \sin\alpha \cos\beta - \frac{W_\theta^2}{r} - \omega^2 r - 2\omega W_\theta \tag{10a}$$

$$-\frac{1}{\rho}\frac{\partial P}{\partial \theta} = W_m \frac{dW_\theta}{dm} + \frac{W_\theta W_r}{r} + 2\omega W_r \tag{10b}$$

$$-\frac{1}{\rho}\frac{\partial P}{\partial Z} = W \cos\alpha \cos\beta \frac{dW_m}{dm} - \frac{W^2 \cos^2\beta \sin\alpha}{r_c} \tag{10c}$$

The above equations are simply expressions of Newton's second law and are assumed to hold along any streamline within the fluid. The equation of the inviscid tangential force [Eq. (10b)] is regarded as the most significant since it exhibits the primary effect of the impeller on the fluid in imparting a rotary motion by means of the tangential pressure gradient between the blades. This equation can be simplified by assuming that $(\partial P/\partial\theta \approx \Delta P/\Delta\theta)$, then the distribution of the parameter $(\Delta P/\Delta\theta)$ along the mean streamline can be calculated (in a step-by-step manner) from the prescribed velocity distribution and the basic geometry of the mean streamline. This corresponds physically to the assumption of an infinite number of blades.

The present calculations have shown that the detailed blade shape is highly sensitive to the variation of radial component of the meridonal velocity. This allowed the meridonal profile itself to be used as a control to the blade shape for any loading distribution. The detailed effects of the above-mentioned parameters will be discussed in the following sections.

The inviscid differential pressure rise along the impeller mean flow line could be written as follows:

$$dP = \rho\{[(W_\theta^2/r) + 2W_\theta\omega + \omega^2 r]\, dr - W_r\, dW_r + W_z\, dW_z\} + (\Delta P/\Delta\theta)\, d\theta \tag{11}$$

The differential pressure in the above equation may be evaluated for each interval along the flow path because all quantities are now known. Having found the total pressure rise from the impeller inlet to outlet by summation of "dP" from Eq. (11), the calculated value has to be corrected by including the loss in stagnation pressure along the chosen flow path. Experience with analyzing few impellers having known geometrical and flow details has shown that the values of "$\Sigma\, dP$" found from the above equation should be multiplied by a factor of 73–82% (fudge factor) in order to check test values [this is because the pressure calculated using Eq. (11) is the inviscid pressure]. Although more complex expressions for calculating the actual pressure rise are available (include surface friction, diffusion effects, curvature effects, etc., e.g., Refs. 14–16), it was decided in this study however, to depend directly on the inviscid estimates based upon Eq. (11). This equation is believed to have the advantages of convenience and of clearly showing the fundamental design components which contribute to the pressure rise. For example, the combined term $(\rho W_{z+r}\, dW_{z+r})$ is the pressure rise due to the fluid flow through the impeller neglecting the effects of the blades (i.e., it represents the impeller as an annular diffusing passage), and therefore, directly shows the effect of changes in the shape of the axial-radial cross section. The last term shows the direct action of the blades in pushing on the fluid and it is the only term which would exist in a purely axial flow fan with constant axial velocity.

The pressure distribution for both blade surfaces is calculated using the approximation that the pressure varies linearly from blade-to-blade, thus

$$P_s = P \pm (\Delta P/2) \tag{12}$$

where the two values of P_s are the surface pressures and ΔP represents the pressure calculated as described by Eq. (10b).

As a result of boundary-layer separation on one or several impeller walls, a zone arises which is dominated by the kind of flow described by Ref. 17. In this zone a low-loss fast jet and a slow-flowing area of wake run side-by-side. Several criteria have been examined for determining the point at which this wake formation begins. It was found that this main separation is best defined by a criterion based on experimental investigations of Ref. 18 and a load coefficient derived in Ref. 19 that have the following form:

$$C_n = \frac{1}{2}\frac{P_p - P_s}{(\rho/2)W^2} \tag{13a}$$

The loading coefficient given by Eq. (13a) is equal to half the difference of the static pressures on the pressure and suction sides of the blade; related to the mean dynamic pressure it can also be written as

$$C_n = \frac{W_s - W_p}{[(W_s + W_p)/2]} \tag{13b}$$

which equals the difference of the relative velocities between the suction and pressure sides of the blade, related to the mean velocity. Based on the experimental findings of Ref. 18, it was found that the critical value of this parameter (where separation is likely to begin) is approximately equal to 0.7, this condition can be stated mathematically as

$$(C_n)_{\text{Limiting}} \leq 0.7$$

The approximate method used to evaluate the relative velocity distribution along the driving and trailing face of the impeller is based on the fact that zero circulation should exist around a closed path (not cutting the vanes). Therefore, the loading coefficient [given by Eq. (13b)] together with the assumption of zero circulation (of an ideal irrotational flow) could be used to mathematically describe the zero circulation condition around an element of the blade passage between two close radii (assuming the whole passage as consisting of

mainly two parts) as follows:

$$\frac{W_p}{\cos \beta_p} - \frac{W_p}{\cos \beta_s} + U(\tan \beta_p - \tan \beta_s) + \sin \alpha \frac{\mathrm{d}}{\mathrm{d}r} \cdot (U + W \sin \beta)b = 0 \quad (14)$$

Where β is the blade angle measured from radial direction (positive for forward-swept impeller).

The value of angle β_p at any point along the mean streamline (of a perfectly guided fluid) could be approximated using the following simplified relation:

$$\beta_p = 2\beta - \beta_s \quad (15)$$

The velocity at the pressure and suction sides can now be evaluated using Eqs. (13b) and (14). The last term in Eq. (14) is found from the slope of the curve $[(U + W \sin \beta)b/\sin \alpha]$ against r. The calculation of the relative velocity distribution along the vane surfaces will serve to highlight the possible regions where local deceleration rate is high and boundary-layer separation may occur. These tendencies could be remedied by the present design procedure (because of its modular structure) by allowing the violation of some inequality constraints in order to delay the areas of possible flow separation without effecting the overall diffusion ratio of the impeller.

The above-mentioned governing equations combined with the continuity of flow equation can be used to calculate the detailed impeller geometry (using a prescribed diffusion rate). The construction of the design program is based on a step-by-step calculation procedure.

Results

The findings that were obtained from using the above-mentioned procedure to design high-pressure ratio centrifugal impellers will now be presented.

Figure 6 shows the front view of two impellers that can theoretically fulfill the same design requirements. The blade shape in the axial view of the initially used velocity schedules (chosen with highly irregular spatial rate of diffusion) along the impeller three basic streamlines (hub, mean, and shroud) has the undesirable effect of having a backward curvature at the leading edge and impeller exit, and a forward curvature at the middle portion of the blade element. This sort of blade curvature in addition to being highly undesirable from the manufacturing point of view is also unacceptable from the spatial rate of diffusion of the relative velocity from inlet to the outlet of the impeller channel. In addition, the blade wrapping in the initial design is considerably greater than in the modified design. The degree of blade wrapping and the detailed shape of the modified design is superimposed on the initial design, and is also shown in Fig. 6.

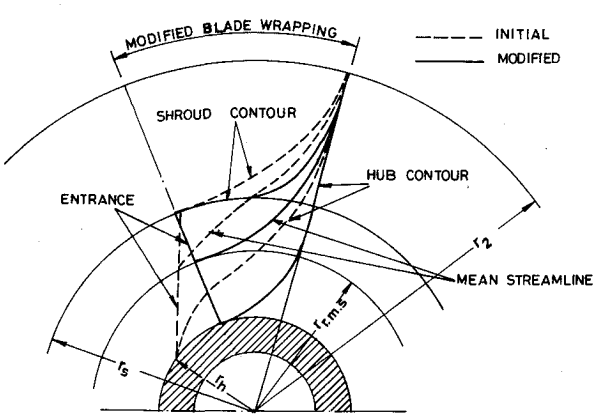

Fig. 6 Front view of a blade element at an initial and modified design stage.

It should be mentioned here that the procedure used to obtain the wrapping angle (based on the available information) was achieved using the following steps: 1) obtain the meridional profile of the impeller from the known hub and shroud radius distribution along the axial length; 2) draw a line at a given radius parallel to the axis of rotation (in r-z plane); 3) project the meridonal section at that radius; 4) calculate blade angles at a chosen radius for different values of the axial length; 5) construct blade centerline profile (mean streamline); and 6) measure the wrap angle between the two extreme values of blade angle which is calculated using the following simple relation:

$$\beta = \text{const/radius}$$

where the const in the above expression is defined by the initial specification of the rms blade angle and radius.

The initial backward curvature was successfully eliminated in the modified design by proper adjustment of the radial and axial variation of the components of relative velocity along the axial length of the impeller (without altering the overall diffusion ratio). The design procedure also succeeded in reducing the blade wrapping which should in radial impellers be as small as possible (for the ease of manufacture, stress considerations, and levels of pressure distribution on the hub and shroud). A preliminary work on several velocity schedules has revealed that the radial-axial component of the relative velocity should have an almost axial entrance and should turn around gradually as it passes through the impeller channel (which also serves to avoid high diffusion rate while turning the flow from axial to the radial direction) and then attains as radial a direction as possible at the impeller exit. The basic component distribution of the prescribed relative velocity of the modified design along the nondimensional mean streamline are shown in Fig. 7. The figure reveals that the highest rate of diffusion was accomplished in the inducer part whereas the radial portion was relatively lightly loaded. Figure 8 shows the characteristics of the meridional velocity schedule that was finally employed so that the undesirable blade curvature (shown in Fig. 6) was successfully eliminated. The various trial distributions that were examined during the design sequence (satisfying the same boundary values), are also shown in Fig. 8.

The blade-angle distribution of the modified design is shown in Fig. 9. The hub, mean, and shroud blade-angle distribution is shown. The designed, modified blade element is of the radial type and turns completely radial at approximately 68.7% of the impeller axial length along its axis of rotation.

Figure 10 shows the pressure loading parameter variation along the nondimensional axial length ratio of the initial and

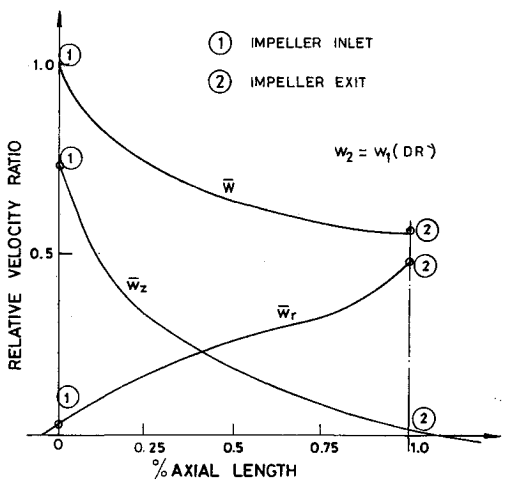

Fig. 7 Prescribed velocity distribution of the modified design along mean streamline.

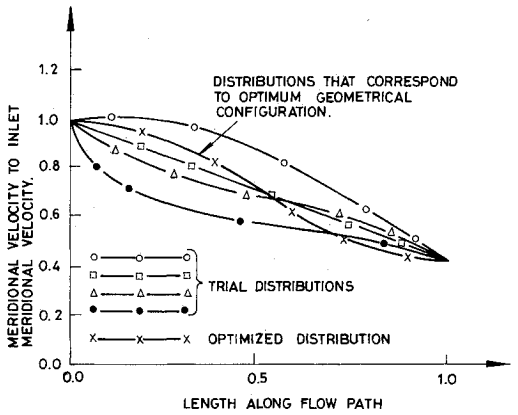

Fig. 8 Progress of the choice of relative meridional velocity.

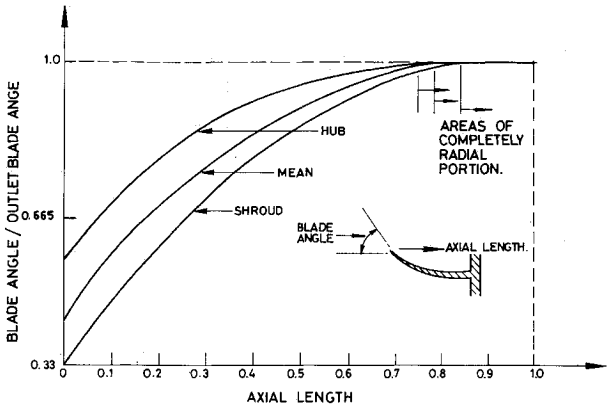

Fig. 9 Blade-angle distribution of the example design.

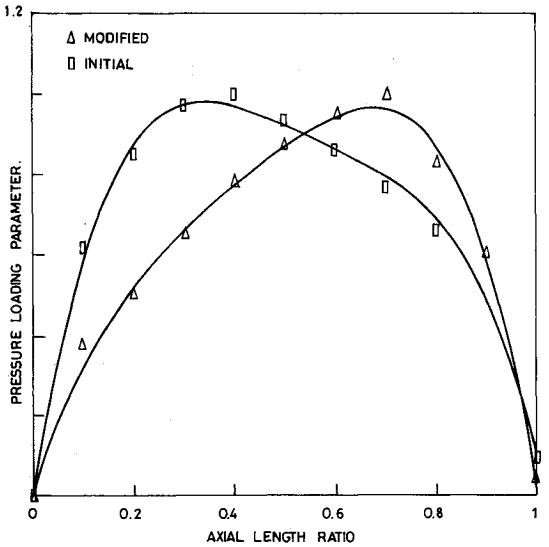

Fig. 10 Loading distribution of the initial and modified design.

the modified designs. It can be seen that for the modified design that the force on the fluid at entrance is zero, then it increases to a more or less uniform maximum (at the approximately middle value of the length along the streamline under consideration) and then it decreases to a small value at the impeller exit. In doing so, the objective of a highly loaded inducer and lightly loaded radial portion has been achieved; in addition no portion of the blade element has escaped its proper share of work. This type of loading distribution has also contributed to the elimination of the undesirable shape of the blade which was shown in Fig. 6.

The geometry generated for the design example has been finally analyzed using the flow analysis program proposed by

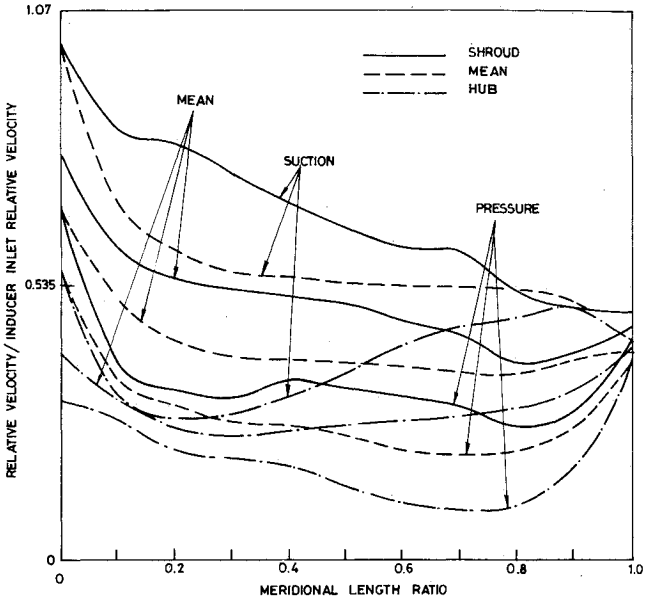

Fig. 11 Velocity distribution along shroud, mean, and hub (mean plane) of the example design.

Katsanis and McNally[20] and is shown in Fig. 11. It can be observed that the velocity deceleration in the mean plane was properly controlled to avoid a possible early flow separation.

Conclusions

A direct-design method for centrifugal impeller blading has been presented. The detailed blade shape is found to be very sensitive to the distribution characteristics of meridional relative velocity and subsequently the blade loading. The method correlates the overall passage contour (as projected in the axial-radial plane), blade shape and diffusion schedules. The effect of various parameters such as level of blade loadings, shape, and the spatial diffusion rate of velocities on a specific design has been determined. Moreover, upon the comparison of the obtained shape and velocity distribution of the example impeller with available geometrical and flow data of impellers with similar capabilities (design mass flow, total-to-total pressure radio, and rotational speed) the obtained impeller did fall within the same general category of existing impellers that are known to have relatively high efficiencies and a satisfactory margin of operating conditions. It was also possible on some occasions (using the proposed method) to explain differences in performance among various impellers which seemed alike on a careful qualitative inspection.

References

[1]Al-Zubaidy, S. N., "Comparative Study Between Different Design Methodologies for Centrifugal Impellers," Society of Automotive Engineers, Paper 891759, Milwaukee, WI, Sept. 1989.

[2]Al-Zubaidy, S. N., "Toward Automating the Design of Centrifugal Impellers," *Proceedings of the Fluid Machinery Forum*, American Society of Mechanical Engineers, Book H00601, Vol. 96, New York, 1990, pp. 41–47.

[3]Schorr, P. G., Welliver, A. D., and Winslour, L. J., "Design and Development of Small, High Pressure Ratio, Single Stage Centrifugal Compressor," *Advanced Centrifugal Compressors*, American Society of Mechanical Engineers, New York, 1971, pp. 147–217.

[4]Musgrave, D. S., "The Prediction of Design and Off Design Efficiency for Centrifugal Compressor Impellers," *Proceedings of the 25th International Gas Turbine Conference and the 22nd Annual Fluids Engineering Conference*, American Society of Mechanical Engineers, New York, 1980, pp. 185–189.

[5]Schumann, L.F., and Clark, D. A., "Effect of Area Ratio on the Performance of a 5.5:1 Pressure Ratio Centrifugal Impeller," American Society of Mechanical Engineers Paper 86-GT-303, New York, June 1986.

[6]Came, P. M., "The Development, Application and Experimental Evaluation of a Design Procedure for Centrifugal Compressors," *Proceedings of the Institution of Mechanical Engineers*, London, Vol. 192, No. 5, 1978, pp. 49–67.

[7]Mashimo, T., Watanabe, I., and Ariga, I., "Effects of Fluid Leakage on Performance of a Centrifugal Compressor," American Society of Mechanical Engineers Paper 78-GT-143, New York, Dec. 1977; see also *Journal of Engineering for Power*, Vol. 101, No. 3, 1979, pp. 337–342.

[8]Rodgers, C., "Impeller Stalling as Influenced by Diffusion Limitations," Transactions of the American Society of Mechanical Engineers, *Journal of Fluid Engineering*, New York, Vol. 99, No. 2, 1977, pp. 84–97.

[9]Eckdart, D., "Detailed Flow Investigation Within a High Speed Centrifugal Compressor," Transactions of the American Society of Mechanical Engineers, *Journal of Fluid Engineering*, New York, Vol. 98, No. 3, 1976, pp. 390–401.

[10]Osborne, C., Runstadler, P. W., and Stacy, W. D., "Aerodynamic and Mechanical Design of an 8:1 Pressure Ratio Centrifugal Compressor," NASA CR-134782, Contract NAS3-17848, April 1975.

[11]Coppage, J. E., Dallenbach, F. E., Chenberger, H. P., Halavake, G. E., Knoernschild, E. M., and Van Le, N., "Study of Supersonic Radial Compressors for Refrigeration and Pressurization Systems," WADC TR 55-257, ASTIA Document No. AD 110467, Contract AF 33(616)-2318, OH, Dec. 1956.

[12]Dallenbach, F., "The Aerodynamic Design and Performance of Centrifugal and Mixed Flow Compressors," Society of Automotive Engineers, Technical Progress Series, Warrendale, PA, Vol. 3, 1961, pp. 2–30.

[13]Balje, O. E., "Loss and Flow Path Studies on Centrifugal Compressors," American Society of Mechanical Engineers Transactions, New York, *Journal of Engineering for Power*, Vol. 92, No. 3, 1970, pp. 275–299.

[14]Herbert, M. V., "A Method of Centrifugal Compressor Performance Prediction," *Proceedings of the 5th International Gas Turbine Engineering Conference and the 22nd Annual Fluids Engineering Conference*, American Society of Mechanical Engineers, New York, 1980, pp. 171–183.

[15]Pampreen, R. C., "Small Turbomachinery Compressor and Fan Aerodynamics," Transaction of the American Society of Mechanical Engineers, New York, *Journal of Engineering for Power*, Vol. 95, Series A, No. 3, 1973, pp. 251–256.

[16]Balje, O. E., "A Flow Model for Centrifugal Compressor Rotars," Transactions of the American Society of Mechanical Engineers, New York, *Journal of Engineering for Power*, Vol. 100, No. 1, 1978, pp. 148–158.

[17]Dean, R. C., "The Fluid Dynamic Design of Advanced Centrifugal Compressors," Creare Inc., TN-185, Hanover, NH, July 1974.

[18]Hill, P. G., and Moon, J. M., "Effects of Coriolis on the Turbulent Boundary Layer in Rotating Fluid Machines," Rept. 69, Massachusetts Inst. of Technology, Gas Turbine Lab., Cambridge, MA, 1962.

[19]Morris, R. E., and Kenny, D. P., "High Pressure Ratio Centrifugal Compressors for Small Gas Turbine Engines," *Advanced Centrifugal Compressors*, American Society of Mechanical Engineers, New York, 1971, pp. 118–146.

[20]Katsanis, T., and McNally, W. D., "Revised FORTRAN Program for Calculating Velocities on the Hub-Shroud Midchannel Stream Surface of an Axial-, Radial- or Mixed Flow Turbomachine or Annular Duct," NASA TN D-8430, 1977.